Chapter 1

Introduction

This chapter provides a brief overview of different layers of the solar atmosphere, and their temperature structuring. Thereafter, a basic outline of the plasma flows in large scale coronal structures (e.g., quiet Sun, coronal hole, and active region) is described. Considering the magnetic coupling of various layers of the solar atmosphere, mainly mass and energy transport processes are briefly reviewed which are associated with the lower part of the solar atmosphere. We conclude this chapter by describing the motivation behind original research work carried out in the present thesis, and the major scientific ideas in the chapter 3-6 are discussed.

The Sun is the crucial driver of life on the Earth and plays an important role in our lives. The energy in the form of quality sunshine provided by the Sun is one of the major factors of life's survival on Earth. The Sun is a spectral type G2V star having physical characteristics of an average star but its close proximity to the Earth makes the Sun an important part of our studies. It is our own laboratory in the nearest space to study the dynamics of other similar stars and understanding the physics of magnetized plasma. The

various layers of the Sun are intricately related to each other by driving the energetic transients and dynamical plasma processes in its magnetized and structured atmosphere. Thus, multi-layer and multi-height studies of different physical phenomena transporting energy and mass from its lower atmosphere to the upper atmosphere become important area of scientific research. The Sun can be broadly classified into its interior and exterior parts. A brief overview of various layers of the solar interior and exterior is given as follows:

1.1 Interior of the Sun

The interior of the Sun which is opaque and not seen directly through the entire electromagnetic spectrum, can be probed only by neutrinos or by helioseismic waves. It consists of three different layers: Core region at the Sun's center reaching upto $0.25R_{\odot}$ where the energy is produced by thermo-nuclear fusion processes (cf., Fig. 1.1). This process is dominated by the fusion of hydrogen nuclei to form helium, therefore, well known as a proton-proton cycle. Energy is formed in the form of Helium nuclei by this proton-proton cycle. This nuclear fusion reaction releases energy in the form of X-rays and γ-rays (26.2 MeV) and two neutrinos (0.5 MeV) and is shown as:

$$4^1H \rightarrow 4He + 2e^- + 2\nu + 26.7MeV \tag{1.1}$$

These tiny subatomic particles known as neutrinos, having no electric charge, do not interact with the matter and travel at nearly the speed of light, escaping without much hindrance through the solar interior. The energy propagates outwards through radiative and convective zones. The interior of the Sun can be considered in hydrostatic balance taking into account a simplest fact that the outward pressure gradient and inward gravitational

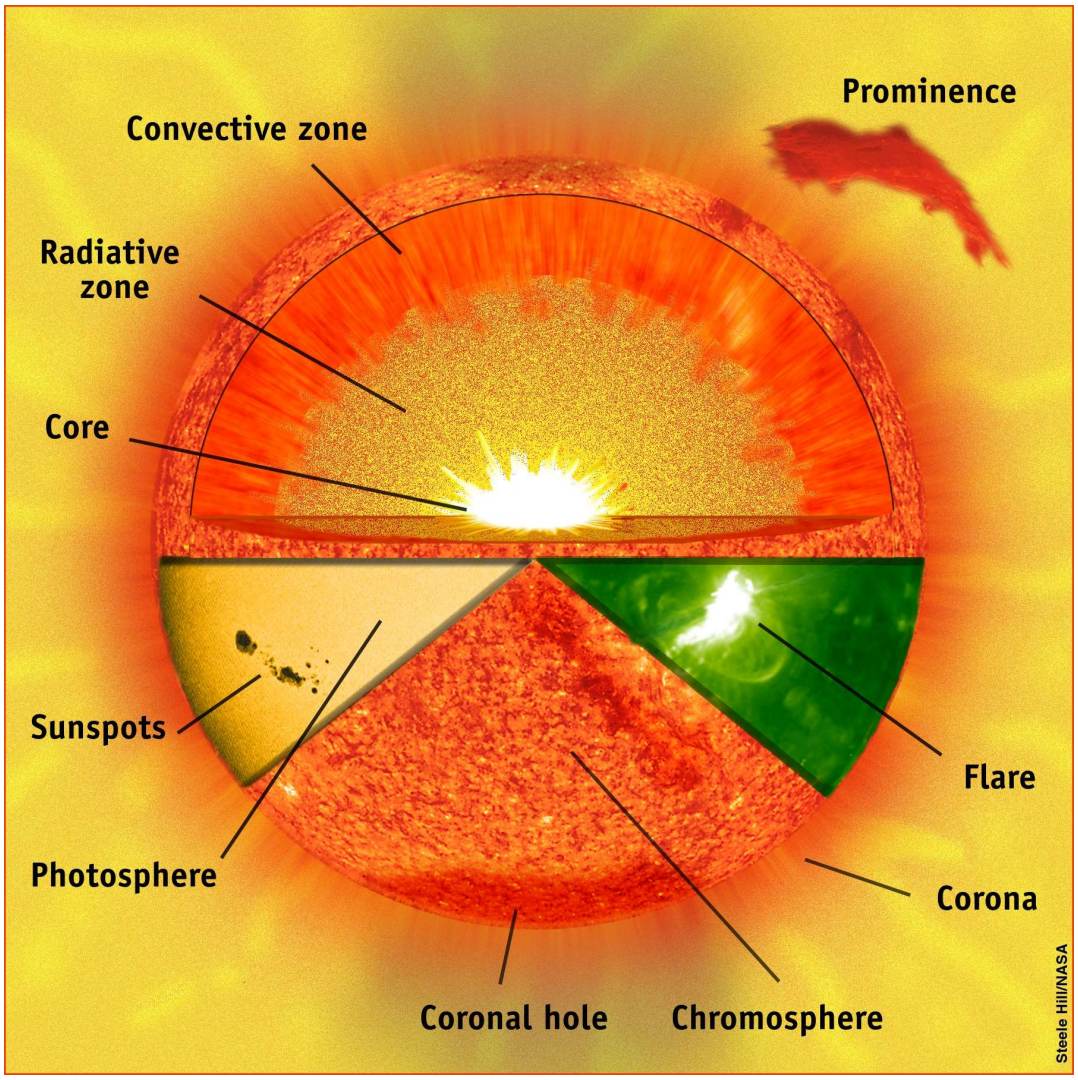

Figure 1.1: This image provides a basic overview of the Sun's parts. The three major interior zones are the core, radiative zone, and convective zone. The core is the innermost part of the Sun where energy is generated by nuclear reactions. The radiative zone is the layer where energy travels outward by radiation through about 70% of the Sun. The convective zone is the sub-surface layer in which convection currents circulate the Sun's energy to the surface. The flare, sunspots and photosphere, chromosphere, and the prominence are all clipped from actual SOHO images of the Sun and overlaid on this particular image. (Courtesy: SOHO, ESA/NASA)

force are balanced by each other at a given radial distance r:

$$\frac{dp}{dr} = -\rho(r)g(r) \tag{1.2}$$

,where $'p'$ is the pressure, $'\rho'$ is the density, and $'g'$ is the gravitational acceleration varying with outward radial distance $'r'$. Also, the plasma is considered to be in radiative equilibrium in the radiative zone ranging from 0.25 $R_\odot$ to 0.7 $R_\odot$. So, the energy is radiated through thermal radiation process in this zone and new ions begin to form by electron recombination of the particles causing opacity and magnitude of temperature gradient to increase. Plasma gas in a radiative zone is denser, therefore, photons generated by nuclear fusion at the Sun's core can travel only a short distance before they are absorbed or scattered by another ion thus making its mean free path very small. These photons take about $\approx 10^5$ years from the core of the Sun to leave the radiative zone, and within this range the temperature is also lowered from 15 MK at the solar core to 1.5 MK upto the base of the convective zone. Moreover, due to the large enough negative density gradient and a net inward buoyancy force, the radiative zone remains stable against the overlying convective zone.

At about 0.7 $R_\odot$, the convective zone starts ranging out where the turbulent convective motion begins to take place. The opacity reduces as we move out causing huge temperature gradient and convective instability to set in. So, the radiation then comes out upto the surface through convective motions in the convective zone. This motion appears as the solar granules which is the photospheric manifestation of the convective motions underneath the surface. At the surface, the radiation escapes through due to insufficient opacity to hold it inside. These three layers thus comprise of the interior of the Sun. The convective motions appear on the surface of the Sun. The magnetic fields also seed in the interior of the Sun. It waxes and wanes at the solar surface, i.e., photosphere, dynamically and permeates to

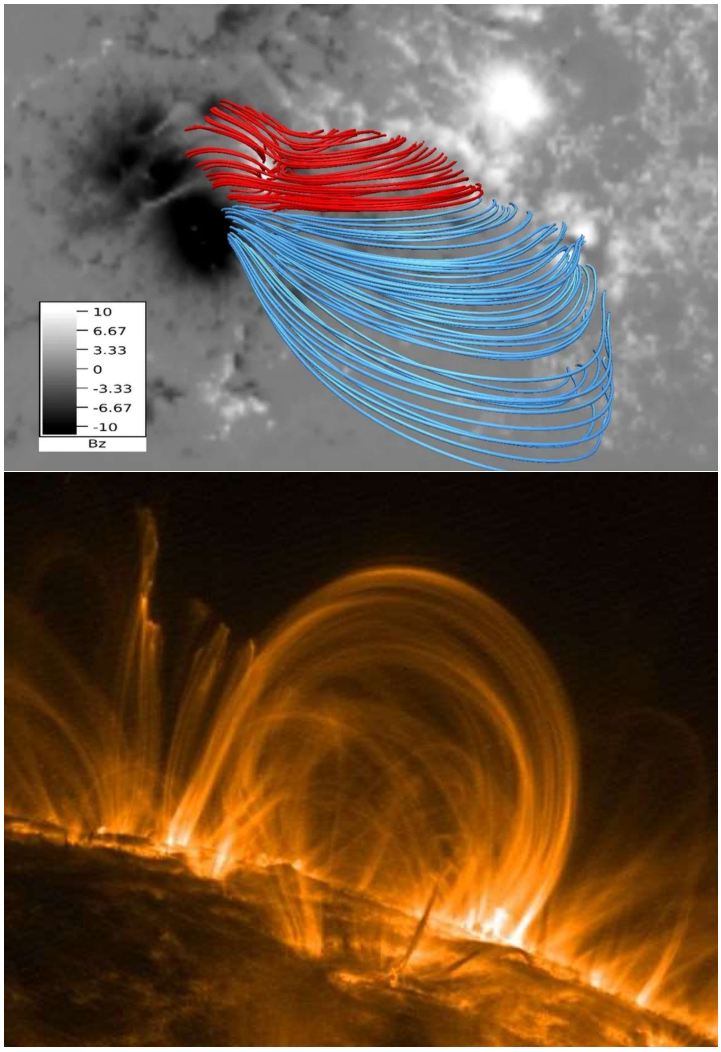

Figure 1.2: Top-panel: The Solar Dynamics Observatory (SDO)/Helioseismic and Magnetic Imager (HMI) vector magnetogram showing a solar active region AR 12192 and its sunspot groups on October 24, 2014 at 21:10 UT. To infer the large-scale coronal magnetic field, a non-force-free field (NFFF) extrapolation is shown overlaid on the pair of sunspot mimicking large-scale closed magnetic field lines (Courtesy: A. Prasad et al., IAUS 340, 2018). Bottom-panel: The active region magnetic loops are shown above the solar-disk as observed by Transition Region and Coronal Explorer (TRACE) on 28th September 2000. (Courtesy: M. Aschwanden; LMSAL; TRACE, and NASA)

the higher atmosphere. In the next sub-section 1.2, we briefly introduce about the active region and quiet Sun magnetic fields.

1.2 Brief Overview of the Sun's Magnetism

Another significant aspect of the solar interior is the generation of the Sun's magnetic field, which fanout in the outer atmosphere and couple its various layers to control the dynamics at diverse spatio-temporal scales (cf., Figs. 1.2 and 1.3). A dynamo process operating at the interface between the convective and the radiative zones is most likely considered to be the source of the solar magnetic field (e.g., Charbonneau, 2005). Strong azimuthal or toroidal magnetic fields generated by the dynamo in the overshooting convective zone encounter a magnetic buoyancy and related instabilities. Therefore, the magnetic fluxtubes rise through the convection zone and emerge at the solar photosphere in the form of bipolar magnetic fields (e.g., Solanki et al., 2006), which finally form the loop structures filling into the corona as its building blocks (Figs. 1.2 and 1.4). The locations where the footpoints of these loops anchor the photosphere are visible either as sunspots or as faculae (cf., bottom-panel in Fig. 1.2 and bottom-part of Fig. 1.4). The upper layers of the coronal loops radiate at extreme ultraviolet (EUV) and X-ray wavelengths (cf., X-ray corona in bottom part of Fig. 1.4 and EUV loops in bottom-panel of Fig. 1.2), thus forming the major radiative emissions from the solar corona. The active region magnetic field associated with the sunspots is of the order of 1000 Gauss, while the plage regions have a typical magnetic field around 100 Gauss. In contrast to the strong amplitude of these magnetic regions, they cover a very tiny fraction of overall magnetic elements present on the solar surface.

Apart from large-scale active region loops, another magnetic features that appear in the quiet Sun are the internetwork elements located in the interiors of the supergranular cells (cf., Fig. 1.3). The quiet Sun exhibits a repetitive pattern of intense kilo Gauss (kG) fields called the magnetic network lying at the boundary of such supergranular cells and a bunch

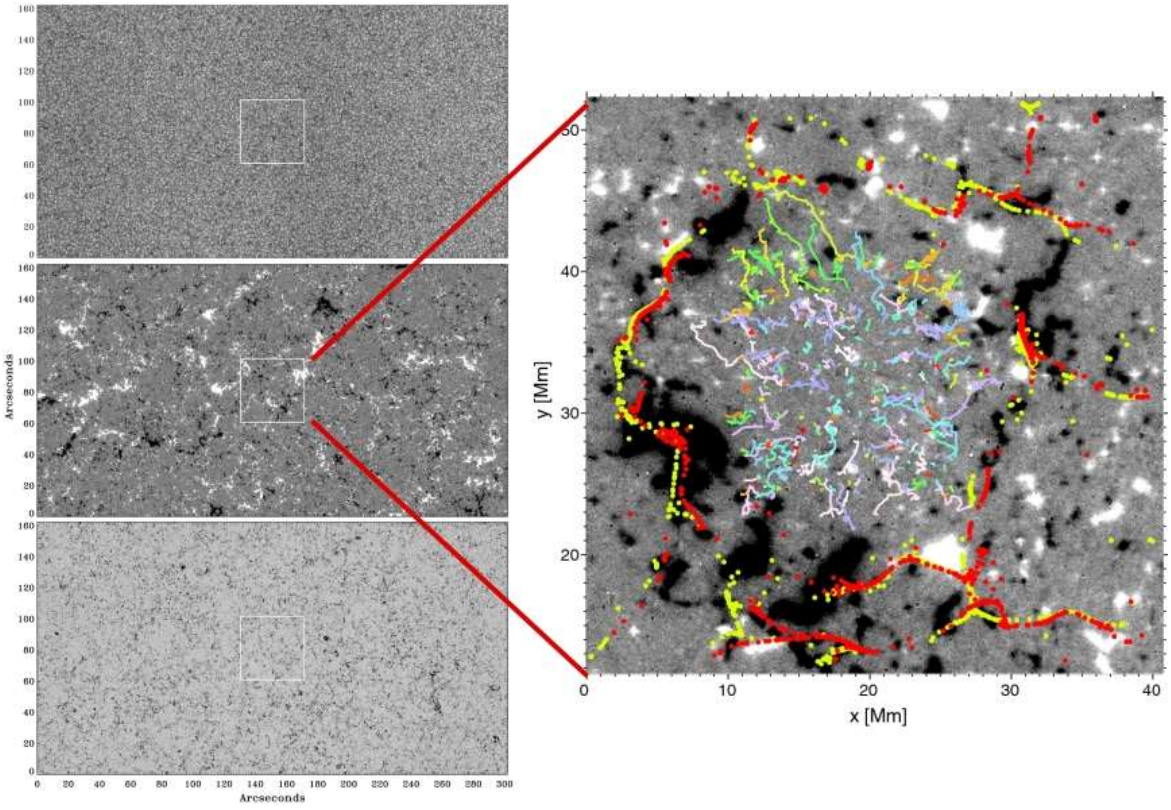

Figure 1.3: Left-panel: Quiet Sun at the disk center as observed by the Hinode spectropolarimeter on 10th March 2007 between 11:37 and 14:37 UT. The top panel shows a continuum intensity map recorded at 630 nm. The other panels display the corresponding maps of longitudinal magnetic flux density (middle) and transverse magnetic flux density (bottom). These images are made using the circular and linear polarization signals as observed in the Fe I 630 nm line pair. Right-panel: Magnetogram showing inter-network magnetic patches within a supergranular cell in a quiet Sun surface. The observations were taken by the Hinode NFI. Different magnetic elements are shown with different colours overlaid on the magnetogram image of supergranular cell. The boundary of the supergranular cell is represented with red and yellow corks that are estimated using respectively the local correlation tracking (LCT) of the continuum intensity and line-of-sight (LOS) velocity structures. The zoomed super-granular cell in right-panel does not hold one-to-one correspondence with the one in the boxed area in left-panel. (Courtesy: Bellot Rubio & Orozco Suárez (2019); Springer Nature)

of weaker and small-scale flux concentrations in the regions in between forming the solar internetwork (e.g., Bellot Rubio & Orozco Suárez, 2019). On a more localized smaller spatial scales in the quiet Sun, the magnetic elements forming faculae and the network, and also appearing in the internetwork regions (cf., boundary and vicinity of the supergranular cell in right-panel of Fig. 1.3), are concentrated in the downflow lanes between granules, (e.g., Bellot Rubio & Orozco Suárez, 2019; Solanki et al., 2006). Almost 90% of the solar surface is covered with the quiet Sun magnetic elements. Even in the quiet Sun itself, there are the diversity in the magnetic fields and their spatial structuring. The magnetic field also ranges to different scales and strengths at the photosphere (e.g., Solanki et al., 2006) in the quiet Sun region. The strong vertical fields of the order of a few kilo Gauss (kG) are concentrated over small parts of the solar surface mostly located at the network regions of supergranular boundaries (e.g., Lagg et al., 2010). The weaker horizontal fields of strengths 100-300 Gauss, however, cover the interior of a supergranular cell with an ambient field of ≈5 Gauss. These strong fields are concentrated into intense flux tubes or small magnetic elements with diameters of 100 km (e.g., Stenflo, 1973). The field strength gradually decreases as the flux tubes start to expand out from 1500 to 1700 Gauss in the deep photosphere to 1000 to 1200 Gauss in the middle photosphere and 200 to 500 Gauss at the temperature minimum. Also, the ratio (β) of plasma to magnetic pressure is 0.2 to 0.4 in the tubes and so the magnetic field dominates the plasma in such highly magnetized fluxtubes most likely rooted in the network regions. In the neighbouring photosphere $\beta \geq 1.0$.

In this way, the subphotospheric dynamics transport the magnetic fields at diverse spatial scales, and form a variety of magnetic structures (e.g., sunspots, pores, faculae/plage around solar active regions, and the network and internetwork fields of the quiet Sun etc) in the solar atmosphere. The overall magnetism of the solar surface is governed in accordance with an 11-year cycle or with some of its extended features (ESCs), which have now

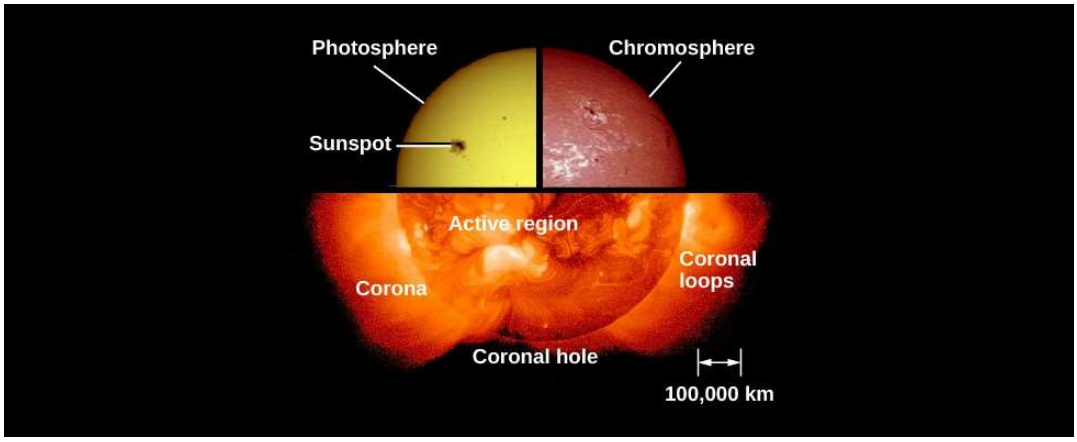

Figure 1.4: A composite image shows the various layers of the solar atmosphere, e.g., the photosphere or surface of the Sun in visible light showing sunspots also, the chromosphere visible in Hα 6563 Å emissions, and the corona as seen in soft X-rays. (Courtesy: NASA)

diverse indicators (e.g., sunspots, giant convective cells, plages and Ca-II K network in the chromosphere, EUV bright-points, 10.7 nm radio fluxes, etc) at the photosphere and even in various layers of the solar atmosphere upto corona (e.g., Hathaway, 2015; Petrovay, 2020; Srivastava et al., 2018b, references cited there). Whatever we observe in terms of the radiation and dynamics of the solar atmosphere is basically the combined manifestation and interplay of the dynamic complex magnetic fields and plasma there. In the next section 1.3, we briefly introduce various atmospheric layers in the exterior of the Sun.

1.3 Atmosphere of the Sun

The atmosphere of the Sun comprises of four different layers which are coupled magnetically with each other. These different layers are explained briefly as under:

1.3.1 Photosphere

The lowermost layer, i.e., surface of the Sun is known as photosphere which appears opaque because of its relatively high density. The surface is seen through the naked eyes

which appear yellow in the visible light (cf., second quadrant in Fig. 1.4). The photosphere of the Sun emits radiation in all the domains of the light dominantly in the visible range and exhibits blackbody radiation curve peaking at ≈5800 K corresponding to yellow light and reaches upto the temperature minimum region where it drops to 4500 K (cf., Fig. 1.5). It hosts a variety of convective processes at different scales such as granulation and supergranulation based on different scales of 1 Mm and 20-70 Mm respectively (cf., Fig. 1.3). However, some weaker motions corresponding to the intermediate scale between granulation and supergranulation and giant cells of scale 200 Mm are also present. These features have plasma flows rising from the center and falling to the edges. In each supergranule cell, plasma rises vertically with a velocity of 30 m s^{-1} in the center, then moving horizontally outwards at 350 m s^{-1} before falling at the boundaries (Hathaway et al., 2002; Rincon & Rieutord, 2018). These irregular shaped cells lasting for a few days keep forming between existing cells or by fragmentation from the existing supergranule. These plasma flows along magnetic fields form strongly diverging areas.

Apart from this quiet Sun dynamical scenario, the manifestation of the active regions appear at the photosphere is the group of sunspots (cf., Fig. 1.4 and 1.6). These dark spots are the regions of large magnetic fields of the order of 1000 Gauss. Their size ranges between 5-25 Mm, and temperature is around 4000 K that is lower than the typical temperature of the solar surface, i..e., ≈5800 K. The gradual process of the formation and decay of the sunspots requires few days. The central region of the sunspot is known as umbra which possess a strong vertical magnetic field (cf., Fig. 1.6, lower-right panel). It is surrounded by the comparatively brighter penumbra in which magnetic fields possess strong horizontal component also thus forming the penumbral filaments. Sunspot is associated with the plasma motions (e.g., Evershed effect, penumbral jets, etc) as well as evolution of magnetic waves and shocks/pseudo-shocks (e.g., Evershed, 1909; Felipe et al.,

2010; Grant et al., 2018; Jess et al., 2019; Katsukawa et al., 2007; Khomenko & Collados, 2015; Srivastava et al., 2018a, and references cited therein).

During the decay of the active regions, the mixed polarity or unipolarity plage regions with a typical magnetic field strength of a few hundred Gauss appear at the solar surface. Plage can also be formed due to more stronger sub-photospheric magnetic activities and emergence of small-scale magnetic fluxes. Moreover, the newly developed sunspots which do not possess penumbra are known as magnetic pores with a typical size (diameter) and life-time of few megameter and few hours respectively.

1.3.2 Chromosphere

The chromosphere holds its origin from Latin word meaning "the sphere of colors". This is the second most layer of the Sun's atmosphere having low density stretching upto few thousand kilometers from 500 to 3000 km. The temperature above the minimum region again starts to increase gradually. This temperature transformation thus represents the lower end of the chromosphere. The temperature then increases from 25,000 K to few million Kelvin through thin transition region and the density decreases (Fig. 1.5). This layer appears reddish due to the hydrogen ions from the core burning off when seen during the total eclipse. It is highly non-uniform and dynamic atmosphere which possess exotic plasma flows, jets, shocks, and wave motions. Different emission lines exhibit different characteristics like revealing supergranule boundaries by Ca II K line emission and small-jet like structures known as spicules at the limb using Hα 6563 Å emissions (cf., first quadrant in Fig. 1.4). The complex interaction of plasma with the magnetic field makes this region difficult to study.

The Ca II K line emission from mid-chromosphere shows the bright irregular patterns at the network region of supergranule boundaries. This network keeps thickening up as the magnetic field keeps spreading out as we go higher in the solar atmosphere. It then

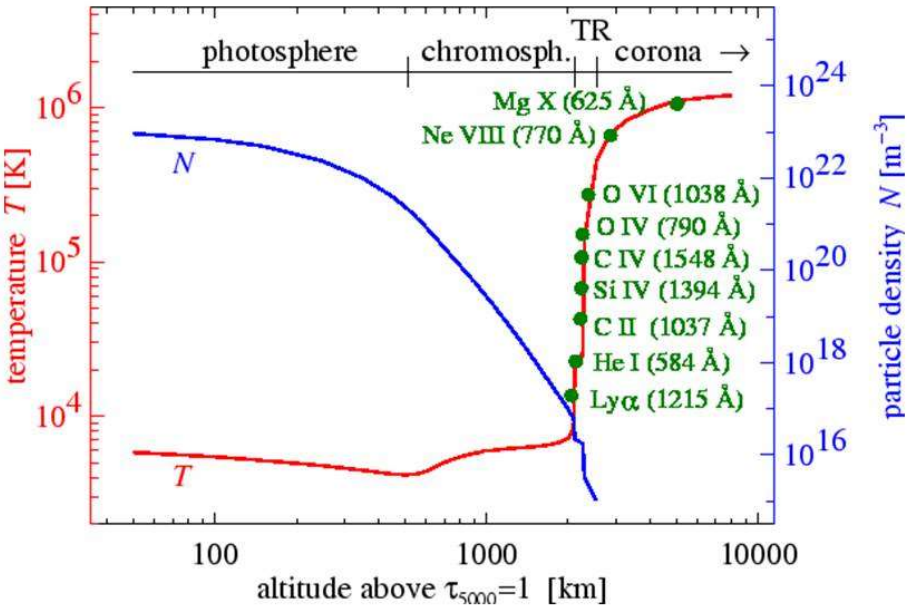

Figure 1.5: An empirical model of the solar atmosphere showing the variation of temperature and density w.r.t height. (Courtesy: Hardi Peter)

vanishes at coronal height temperatures. At the limb, Hα shows densely populated vertical thread like structures known as spicules. They are small scale plasma ejections which keep falling back to the chromosphere as are explained later in this chapter. The plasma β <1 in active regions and $\beta \geq 1$ elsewhere are achieved for chromosphere where magnetic flux spreads. It also merges with a thin static horizontal layer of height 100 km known as transition region which is mainly imaged in the EUV emission lines.

1.3.3 Transition region

The transition region is a thin and irregular layer of the solar atmosphere which is sandwiched between cool chromosphere and the hot corona, and basically acts as an interface

between these two distinct atmospheric layers. In this layer temperature rises abruptly from 20,000 K to 1,000,000 K, while density falls off rapidly (cf., Fig. 1.5). The radiation in the transition region is dominated by the ions with intermediate ionization states (e.g., C IV, O IV, and Si IV, etc) which emit mostly in UV/EUV range, therefore, it can be observed using space-borne UV telescopes only. The width of the transition region varies in variety of magnetic regions, e.g., it lies more higher in the coronal holes compared to the active regions. This acts as a transition layer that causes the reflection and trapping of the magnetic waves, evolution of magnetoacoustic shocks, and controls the mass and energy transport in the localized inner corona.

1.3.4 Corona

The corona holds its origin from Latin word meaning "the crown". This is the outermost layer of the solar atmosphere which is generally dominated by the magnetic fields. In the visible light, it appears as halo of high temperatures and low density during eclipses. So, the corona is mostly observed through creating artificial eclipse by using coronagraph which occult the photospheric light. The halo is seen due to scattering of photospheric light through electrons (K-corona) and dust (F-corona). In the 1940s, many high ionization spectral lines were identified from elements corresponding to the coronal temperature 10^6 K. Due to its high temperature plasma (10^6 K), high ionization lines of known elements are observed and thus, X-rays and UV/EUV are emitted and imaged. This increase in temperature from ≈5800 K at the solar surface to 10^6 K in the corona defying the fundamental law of thermodynamics is a long standing problem known as "Coronal Heating" problem.

The magnetic fields are highly structured in the lower corona which appear as bright coronal loops while the open fields stretch outwards to the outer corona radially along with solar wind. The quiet inner corona has mean electron number density of the orders of

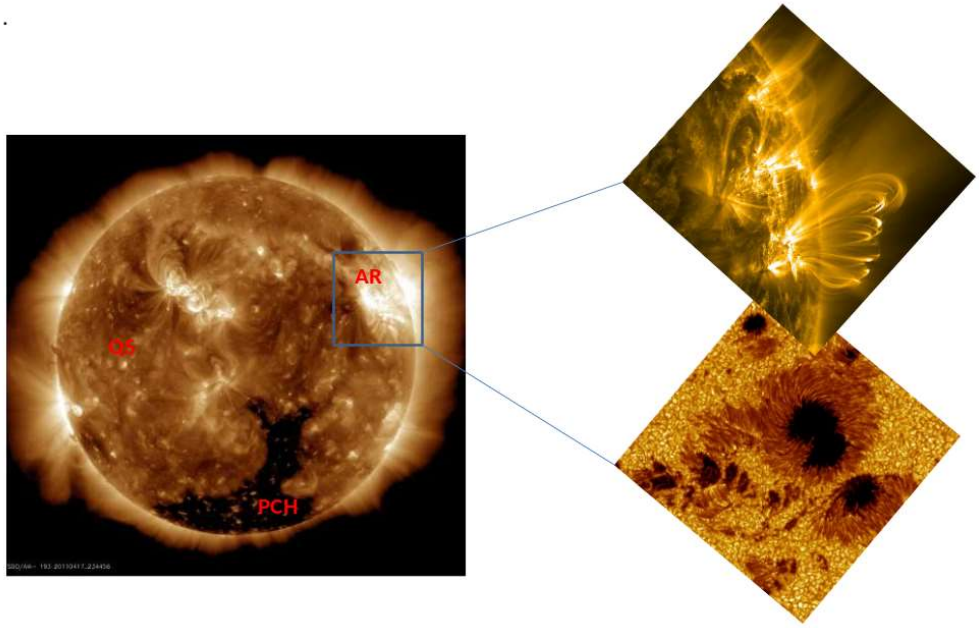

Figure 1.6: The left panel shows the full disk image of the Sun as seen in 193 Å emissions corresponding to the coronal temperature. The different features are then identified as Quiet Sun (QS), Active-region (AR), and Polar Coronal Hole (PCH). The right panel shows the photospheric (sunspots) and coronal (magnetic loops) counterparts of an active region. The zoomed loop system and sunspot groups in the right panel do not possess one-to-one correspondence with the AR shown in the boxed area in left-panel. These image panels are shown just to collectively represent the three major regions (QS, CH, AR) in the solar corona, with an emphasis on AR magnetic loops. (Courtesy: SDO/AIA; SST)

10^{14} m^{-3} (10^{8} cm^{-3}) and it can vary by factor of 5 to 20 depending on various locations. The number density however falls off rapidly with distance from the solar surface which is a few times 10^{12} m^{-3} at 1 $R_{\odot}$ above the surface and less than 10^{10} m^{-3} at 10 $R_{\odot}$. The corona hosts a variety of localized phenomena such as coronal jets, X-ray jets, coronal brightening and large-scale features such as flares, prominences, CMEs etc. Apart from these dynamical processes, the coronal magneto-plasma system also serves as magnetohydrodynamic (MHD) waveguides, and support the evolution of variety of wave modes and their oscillations.

The solar corona may be classified broadly in three regions (cf., Fig. 1.6), namely, (i) Quiet Sun (QS); (ii) Coronal Hole (CH); and (iii) Active Region (AR) (Aschwanden, 2005). These magnetic structures serve as a suite for the violent solar eruptions, waves and oscillations, and large-scale plasma flows and jets. In the next section 1.4, we briefly summarize the state-of-art developments on understanding the large-scale plasma flows in these regions, and thereby determining their role in mass transport to the nascent solar wind.

1.4 Large-scale Plasma Flows in the Different Regions of the Solar Corona

Our studies in this thesis predominantly focuses on UV/EUV emissions from the Sun. In the visible light, the Sun appears to be continuum emission of yellow light with few dark spots known as sunspots or active regions (ARs) where the bipolar coronal loops are anchored. The UV emission shows the continuum bright emission of quiet Sun with its magnetic elements. The dark regions with reduced UV and X-ray emissions are characterized as coronal holes (CHs), which possess the open field lines. The active regions appear as small patches of complex structured very bright emissions having high energy which emits in X-rays as well. These different regions host plasma flows corresponding to different features in the solar atmosphere which are described as below. The Fig. 1.6 shows the different regions (QS, CH, and ARs) in the corona showing their morphological magneto-plasma structuring and relative extent of EUV emissions, thus brightness.

1.4.1 Flows in the quiet Sun and coronal holes

The quiet Sun (QS) is the region dominated by bright emission in the EUV lines as shown in the left panel of Fig. 1.6. The QS is comprised of small-scale loop-like EUV bright points, open magnetic funnels that may be the lower part of the large-scale quiescent

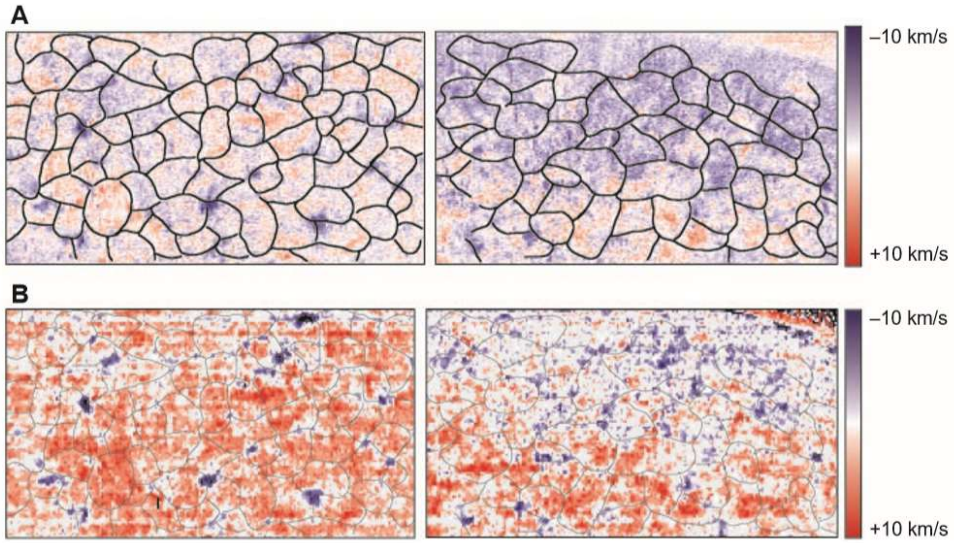

Figure 1.7: SUMER Ne VIII 770 Å line-of-sight Doppler velocity images from the midlatitude region (left), and the polar region (right) of the Sun. The chromospheric network boundaries are superimposed over the Doppler maps. The top images as displayed in 'A' are fitted and derived using a moments technique on unbinned data and used off-limb solar observations to provide the 'zero' velocity reference. The bottom two images as displayed in 'B' are obtained using Gaussian fitting routines on binned data to increase the signal-to-noise ratio. The details of the observational data and scientific results shown in this picture are described by Hassler et al. (1999). (Courtesy: SoHO/SUMER; ESA/NASA; D.M. Hassler)

coronal loops, and low-lying network loop systems. Coronal holes are the regions having low density with open magnetic fields and are characterized by dark region (Fig. 1.6, left panel) in the UV/EUV emissions (Cranmer, 2009) making it distinguishable from surrounding regions. Coronal holes give rise to the solar wind through open diverging magnetic structures even though the magnetic field is quite low (≈1-2 Gauss). Although, coronal holes are generally dominated by strong unipolar polarities with typical magnetic flux of 10^{23} Mx for an averaged field strength of 5 to 10 Gauss. Some elongated structures (polar plumes or coronal rays) are clearly visible at polar coronal holes during eclipses. It also gives rise to fast solar wind. However, the origin of solar wind still needs to be understood by coupling of multi-wavelength observations.

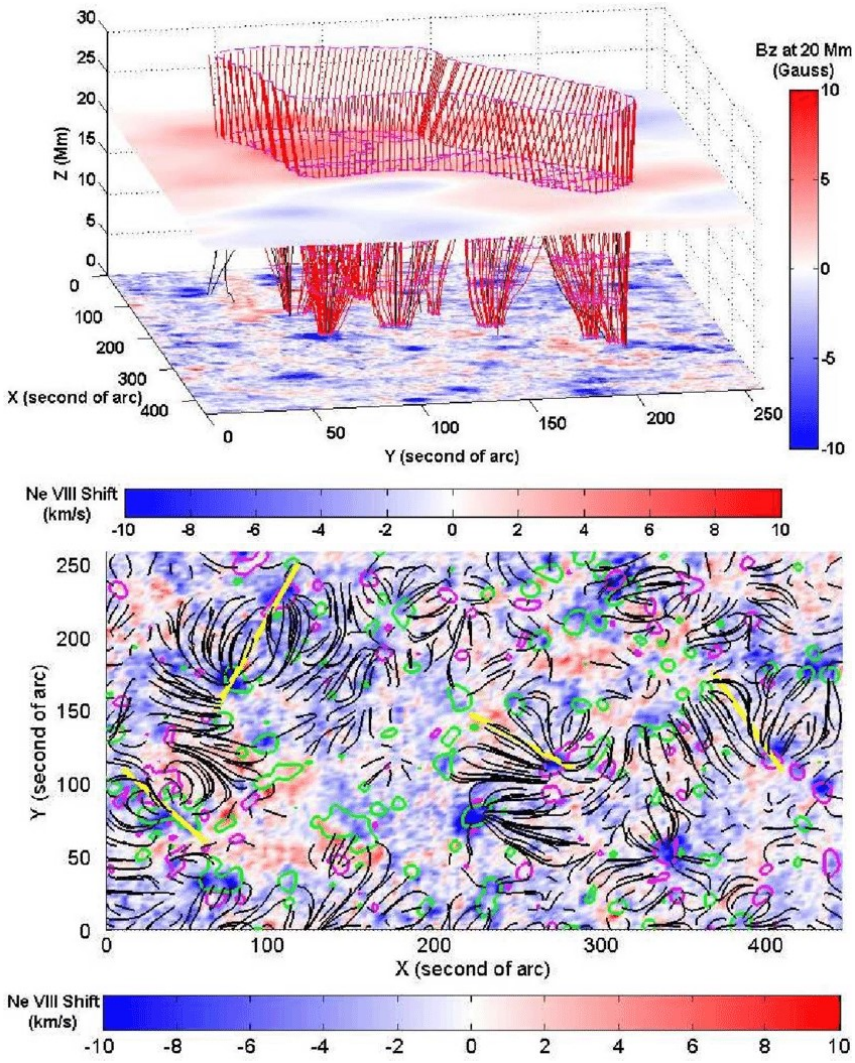

Figure 1.8: Top-panel: Flowing magnetic funnels are shown in a quiet region of the Sun. The magnetic field lines (red) are originating from the funnel boundary, while the black lines are open field lines outside small funnels. The Ne VIII Doppler shift image is placed at zero megameter, and the color coding is given at the bottom. The positive and negative values represent redshifts and blueshifts respectively in the observed Doppler maps. The map of the vertical component of the extrapolated magnetic field at 20 Mm is placed at the height of 20 Mm, and the color coding is given on the right-hand bar. Bottom-panel: Projection of the extrapolated quiescent magnetic loops reaching higher than 4 Mm onto the x-y plane together with the map of the Ne VIII Doppler shift are shown. Regions with positive and negative magnetic flux density are depicted with the green and pink colors, while the contour level of the magnetic fields is given as 15 G and -15 G respectively. The details of the observational data and associated results shown in this image is described by Tian et al. (2009). (Courtesy: SoHO/SUMER; ESA/NASA; Hui Tian).

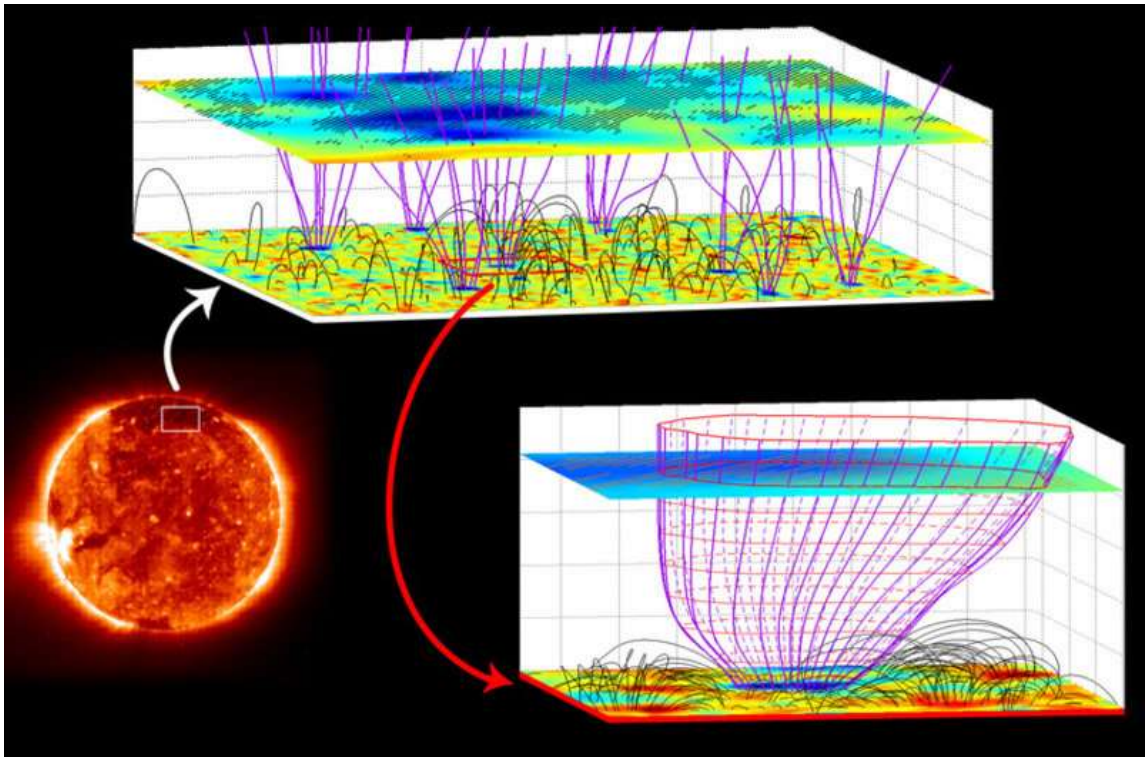

Figure 1.9: This picture is an illustration after Tu et al. (2005) of the solar magnetic transition region, showing the solar disk (left) together with a segment of the coronal magnetic field at the pole (a) and a further zoomed part of that field (b). The magnetic field attains a shape of the rapidly expanding coronal funnel. The open magnetic field lines are drawn in magenta in this funnel. The field strength is indicated in blue on the top plane at a height of 20 Mm. At this height, the outflow speed of the plasma is found to be $\approx$10 km s^{-1} that is indicated by hatched areas. (Courtesy: Marsch (2018); SoHO/SUMER; ESA/NASA)

Earlier, the persistent redshifts by few km s^{-1} were reported in the TR at the network regions of the quiet Sun (e.g., Brekke et al., 1997; Chae et al., 1998c; Curdt et al., 2008; Doschek et al., 1976, and references cited therein). A remarkable improvement occurred in understanding the flow structures of the quiet Sun and coronal holes (Fig. 1.7), which measured the Doppler velocity maps of SUMER Ne VIII 770 Å line for QS (Fig. 1.7 left-panel) and CH (Fig. 1.7 right panel). The overlaid black grid structures are the supergranule boundaries plotted using radiance maps. These results showed the relationship between measured outflow (blueshift) and magnetic network structure. The blue colour represents blueshifts or outflows and red represents redshifts or downflows. The velocity scale represents the darkest red regions corresponding to roughly 10 km s^{-1} redshift and the darkest blue regions corresponding to a 10 km s^{-1} blueshift (Hassler et al., 1999). Ne VIII line formed in the upper TR was found to be blueshifted on average in the quiet Sun as well as coronal holes (Wilhelm et al., 2000). However, Tian et al. (2009) reported that these blueshift locations are not related to the open-field regions and are mostly related to footpoints of the closed loop systems. The QS may be associated with the coronal funnels (Fig. 1.8, top-panel), which also exist in the quiet Sun (Tian et al., 2008). Strong plasma outflow, which can be traced by large Ne VIII blueshift as observed by SoHO/SUMER may not be primarily associated with the solar wind originating in the coronal funnels. However, it is associated with the signature of mass supply in closed magnetic loops at the coronal heights (cf., Fig. 1.8, bottom,-panel).

Another leap forward development is done when Tu et al. (2005) studied the origin of the solar wind in the coronal holes based on the earlier studies of identification of the source region by Hassler et al. (1999) for polar coronal holes and Xia et al. (2003) for equatorial coronal holes. These studies were conducted by correlating the Si II radiance and Ne VIII Doppler velocity maps using solar spectral observations from SoHO/SUMER. Tu et al. (2005) have studied the height where the acceleration of solar wind starts. The plasma

flows at the base of the funnel shaped magnetic configuration for different spectral ions Si II, C IV, and Ne VIII show blueshifts corresponding to the strong radiance map exhibiting upflow which forms at a height of 20 Mm. Also, MDI magnetic field extrapolations have been compared with Doppler velocity structures in coronal funnels. Fig. 1.9 illustrate the studies by Tu et al. (2005) showing the region of magnetic funnel in the coronal holes and the extrapolated magnetic field lines (Marsch, 2018). Using multi-spectral lines from SUMER, they found that Si II has an average downflow speed of 2.0 km s^{-1} at 4 Mm, C IV an almost zero speed of 0.3 km s^{-1}, and Ne VIII a clear upflow speed of 9.6 km s^{-1} at 20 Mm. Therefore, no outflow is found for the carbon. So, they reported that below 5 Mm, mostly horizontal exchange of mass and energy takes place between neighboring flux tubes, which is driven by supergranular motion. Above 5 Mm, vertical transport becomes prominent thereby forming the source of the fast solar wind.

1.4.2 Flows in the active regions

Active regions are formed when the new magnetic flux pushes up from below the photosphere and appears as a group of dark spots surrounded by bright region known as photospheric faculae (cf., Fig. 1.6). These relatively cooler dark spots known as sunspots possess highly concentrated magnetic flux (Fig. 1.6, right panel). Active regions, thus, also appear as Hα plage in the chromosphere and coronal bright loop structures in the corona (Fig. 1.6, top-right panel). The highly-structured arch-shaped magnetic structures visible above the active regions in the corona are known as coronal loops.The fascinating loop structures seen in UV/EUV light are the manifestation of plasma embedded along with the magnetic fields drive different phenomenon such as jets, compact flares, and some times Coronal Mass ejection (CMEs) etc. The loops connect different active regions having typical temperature of 2-3 MK and electron number density (10^{14} - 10^{15}) m^{-3}. The sunspots and the surrounding regions have strong magnetic fields of the order of few kilo

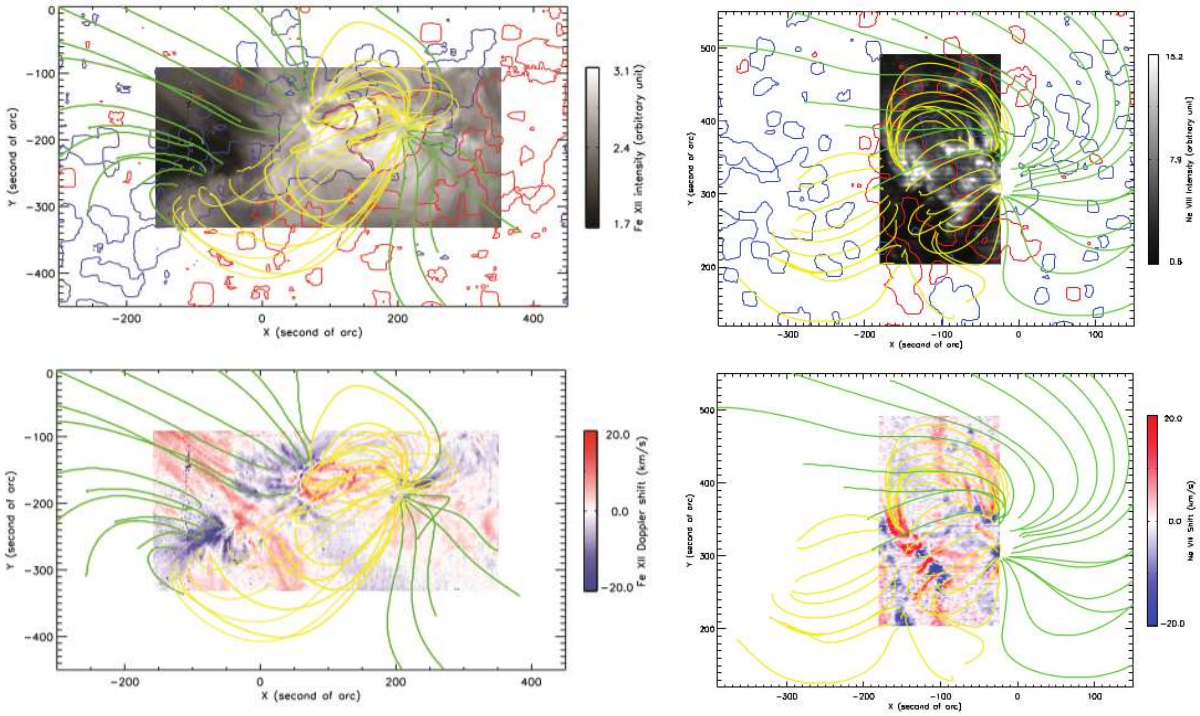

Figure 1.10: Left-Top: EIS Fe XII radiance image in arbitrary units is mapped with various magnetic field lines of the extrapolated coronal magnetic field as shown in the projection. The intensity is displayed on the gray scale as set by the bar on the right side of the given image. The spatial solar coordinates are represented in arcsec. Left Bottom: The EIS Dopplergram of the corresponding Fe XII line shift is shown in the similar format. The velocity scale ranging between -20 and +20 km s^{-1} is defined by the red/blue colour bar at the right side of the given image. Note that the magnetic field lines start and end in patches of predominant plasma flows either in red- or blue-shifts, i.e., footpoints are associated with either up- or down-flows there. Right Top: The SUMER Ne VIII radiance in arbitrary units is mapped with various magnetic field lines of the extrapolated coronal magnetic field as shown in the projection. The magnetic fields represented by green and yellow lines indicate open and closed field lines respectively. The intensity is given in the gray scale set by the bar on the right of the given image. The spatial solar coordinates are given in arcsec. The red and blue contours indicate the field strength at 30 Gauss level for the opposite polarities. Right Bottom: SUMER Dopplergram of the corresponding Ne VIII line shift is displayed in the similar format. The velocity scale ranging between -20 and +20 km s^1 is defined by the red/blue bar at the right side of the given image. It should be noted that the magnetic field lines start and end in patches of predominant flows either red- or blue-shift, i.e., footpoints are associated with either up- or down-flows there. In particular, in the area defined by the intervals x=(-140", -90") and y=(250", 310"), there are locations with adjacent alternating red/blueshifts and varying magnetic connections to mostly the same Doppler shift at both the loop footpoints. The details of the data presented in this figure is described by Marsch et al. (2008). (Courtesy: SoHO/SUMER; Hinode/EIS; ESA/NASA; Hui Tian)

Gauss (kG). The footpoints of these loops are anchored in the islands of strong magnetic field. The plasma flows are mostly dominated by magnetic fields since β <1 for coronal plasma. The thermal properties and diagnostics of loop plasma broadly gets classified into hot, warm, and cool loops. The plasma flows in different loop systems harboured at ARs are of significant importance to study the mass and energy transportation to the outer atmosphere. Coronal loop geometries are specified to infer magnetic fields of the corona.

Kjeldseth-Moe & Brekke (1998) have provided the various evidences of presence of considerable flows at multi-temperature heights in the corona. Winebarger et al. (2002) have studied steady flows in coronal EUV loops and reported intermittent flows in a loop system. Most of these studies presented the redshifts at both the legs of the loops. However, Tian et al. (2009) also showed the blueshifts at the footpoints of the bundle of the loops. Such flows generally attributed to the siphon flows were first reported by Spadaro et al. (2000). The strong blueshifts occur in low-density regions which makes it difficult to observe. Dammasch et al. (2008) revealed steady downflows at transition-region (TR) and lower-corona temperatures. Marsch et al. (2008) have studied the plasma flows guided by strong magnetic field in the solar corona. In the top-left panel of Fig. 1.10, the radiance of EIS Fe XII line is shown along with the extrapolated coronal magnetic field lines. The bottom-left panel shows the Dopplergram of the corresponding Fe XII line shift. The top-right and bottom-right panels show the SUMER Ne VIII radiance map and Dopplergram respectively. The velocity ranges from -20 to +20 km s^{-1} and is shown by colourbar on the right side. The green and yellow lines indicate open and closed field lines, respectively. The red and blue contours indicate the field strength at the 30 Gauss level for opposite polarities. It indicated adjacent upflows and downflows using magnetic field extrapolation. The flows from cool O IV (formation temperature 0.16 MK) and hot Ne VIII (0.63 MK) and Dopplergram of hot Fe XIII (1.3 MK) present the blueshift to be correlated with the open field lines. The blueshifts in O IV and Ne VIII emissions might be related to bulk

plasma flows as was also found in Tian et al. (2009). The association of blueshifts near ARs gave signatures of nascent solar wind (Harra et al., 2008).

In conclusion, the plasma flows in the QS and CH magnetic fluxtubes at coronal heights as it was revealed by coronal spectroscopic observations in the era of SoHO/SUMER and Hinode/EIS in last twenty five years. However, with the advent of Interface Region Imaging Spectrograph (IRIS), a variety of the studies now reveal that the transport of the mass and energy in the TR/Corona is basically linked with localized small-scale reconnection, magnetic waves and associated plasma dynamics in the dynamical chromosphere lying below of it. In the next section, we briefly outline the concept of some significant mass and energy transport processes in the lower part of the solar atmosphere.

1.5 Dynamical Chromosphere

1.5.1 Quiet Sun dynamical plasma processes

The quiet Sun lower solar atmosphere possesses complex magnetic and plasma structuring (Fig. 1.11) and provides a portal for the evolution of localized transients (e.g., small-scale energy release and associated jets/flows) at diverse spatial and temporal scales (e.g., spicules, macrospicules, tornadoes, network jets, cool flowing loops etc). These jets are capable of transporting mass and energy in the overlying atmosphere (e.g., De Pontieu et al., 2004, 2011; Kuridze et al., 2015; Martínez-Sykora et al., 2017; Reid et al., 2016; Samanta et al., 2019; Tian et al., 2014a; Wedemeyer-Böhm et al., 2012, and references cited there). There are also small-scale reconnection processes in the chromosphere/TR and associated energy release, which may lead to hot plasma flows, wave dynamics and their conversion/dissipation, evolution of shocks and associated flows, etc. These are the typical physical processes (cf., Fig. 1.11), which may be responsible collectively for the

localized heating as well as mass transport processes that may couple to the overlying inner corona also.

Spicules are small elongated jet like structures seen at the limb in Hα, and they are typical chromospheric plasma ejecta. Beckers (1972) have first introduced two different types of spicules based on their line profiles and named them as 'Type I' (wide) and 'Type II' (narrow) spicules. De Pontieu et al. (2007a) have then categorized them into two types of spicules on the basis of their fundamental properties: 'Type I' and 'Type II', which seem to have different formation mechanism. The origin of short duration/high velocity spicules (type II) has been attributed to magnetic field reconnection. On the other hand, the origin of Type I, classic spicules (long duration/ low velocities) seems to be associated with the leakage of p-modes into the upper atmosphere and subsequent development of shocks that follow the magnetic field lines (De Pontieu et al., 2004). However, there are a variety of views that these spicules can be originated by waves (Srivastava et al., 2017) and/or reconnection (Samanta et al., 2019). Fibrils and mottles are the on-disk counterparts of the spicules in the active region and quiet Sun, respectively. Most dynamic fibrils have short lifetimes (3-6 mins). This fact is still not fully established, however, many scientific studies support the fact that spicule motions can significantly contribute to the large scale plasma flows in the inner corona and thus transport of mass to the nascent solar wind (e.g., He et al., 2008; McIntosh, 2012; Wójcik et al., 2019, and references cited therein).

One of the main results that have emerged in IRIS era is the discovery of network jets (Tian et al., 2014a). These jets can have a common site of origin to that of the chromospheric spicules, i.e., chromospheric network boundaries where magnetic field concentration is large and intermittent reconnection can occur (Yang et al., 2018). The localized energy release due to the small-scale magnetic reconnection at the boundary of magnetic network is proposed to be a main triggering mechanism for the formation of network jets (Kayshap et al., 2018). There are recent reports that typical chromospheric

spicules are also generated by magnetic reconnection (Samanta et al., 2019). Therefore, how the reconnection phenomena at the similar site can differentiate the origin of spicules and network jets, is still an open question. These thin jet-like structures, initially found in IRIS coronal hole (CH) observations, are termed as network jets and are essentially a transition region phenomenon (Tian et al., 2014a). The network jets were reported with apparent terminal speeds of ≈80-250 km s^{-1}, and were associated with footpoint brightening. Their lifetime ranges from 20 to 80 s, with lengths between 4 and 10 Mm, and average widths of around 300 km (Tian et al., 2014a). Networks jets can also occur in the quiet Sun (QS), however, they are longer and faster in coronal holes (Narang et al., 2016). Kayshap et al. (2018) analyzed 51 QS jets and estimated their mean properties, e.g., apparent speed (140.16±39.41 km s^{-1}), length (3.16±1.18 Mm), and lifetime (105.49±51.75 s). Contrary to previous findings, Kayshap et al. (2018) reported an important physical property of QS network jets that they exhibit rotational motion with a mean velocity of 49.56 km s^{-1}. The morphological feature, length, lifetime and speed of the network jets show some resemblance to spicules, and it is possible that spicules may be heated to TR temperatures (Pereira et al., 2014).

In conclusions, there are a variety of other small-scale cool plasma ejecta, e.g., anemone jets, swirls and tornadoes, macrospicules that may be triggered in the chromosphere/TR and can transport the mass and energy in the overlying corona contributing to its bulk mass flows and formation of the nascent solar wind. At many instances, the rotation/helical twist is evident in some of the samples of these observed chromospheric jets, e.g., associated with swirls/tornadoes, network jets, macrospicules (Kamio et al., 2010; Kayshap et al., 2018; Wedemeyer-Böhm et al., 2012). A reconnection based jet model invokes quite satisfactorily the episodic jet motions which are associated with the twisting or helical motions of their spire (Pariat et al., 2015). As far as newly discovered network jets are concerned, there is less information available on their triggering mechanisms. Yang et al. (2018) have

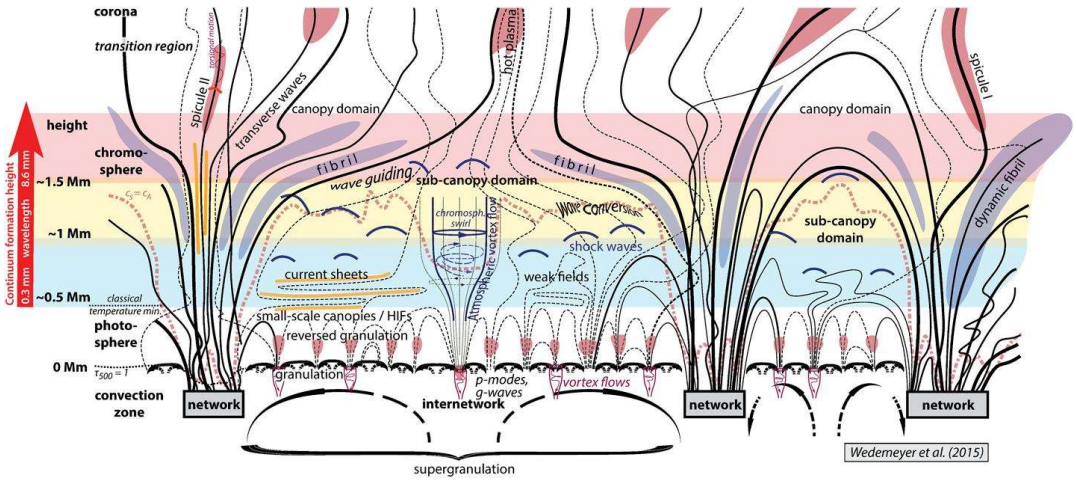

Figure 1.11: Schematic structure of the atmospheric layers in the quiet Sun regions of the solar atmosphere, i.e. in and outside the strongest network magnetic field concentrations, exhibiting a multitude of different physical phenomena. The black solid and dotted lines represent magnetic field lines. The arrow to the left and coloured bars illustrate the height range mapped by ALMA. Aspect ratio is not to scale. (Courtesy: S. Wedemeyer)

reported a numerical model based on magnetic reconnection driven by a combination of magnetic flux emergence and horizontal advection showing that both network jets and spicules can be launched simultaneously in the lower solar atmosphere. The important scientific clues came to light when Chen et al. (2019) found a relation between transition region EEs and their connection to network jets. This implies that the small-scale, localized reconnection may yield some energy burst in the form of such EEs, which can indirectly influence the stable plasma environment to further lead the collimated plasma motions in form of jets. This classical scenario of jet formation is not directly associated with the Lorentz ($j \times B$) force as studied by many authors (e.g., Iijima & Yokoyama, 2017; Martínez-Sykora et al., 2017; Nishizuka et al., 2008, and references cited there). Contrary to this particular scenario, it depicts the onset of plasma pressure (or velocity) perturbations at photospheric/chromospheric heights and thus evolution of the shock-enabled plasma ejecta as an aftermath of localized heating (e.g., Kayshap et al., 2013; Martínez-Sykora

et al., 2009; Murawski et al., 2011; Srivastava et al., 2018a; Suematsu et al., 1982; **?**, and references cited there).

A cutting edge scientific discovery has recently been made using the IRIS spectroscopic observations. Chen et al. (2019) have found that reconnection generated explosive events (EEs) with double peaked Si IV 1393.755 Å profiles or enhancements in both line wings at network lanes, are associated with the footpoints of network jets or transient compact QS brightening. Huang et al. (2014) have also observed typical EEs at subarcsecond scales with strong non-Gaussian profiles and blue- and redshifted velocities of up to 150 km s^{-1} in Si IV 1402.8 Å, Mg II k 2796.4 Å and C II 1334.5 Å lines. These EEs are associated with small-scale plasma ejections, however, they do not fall in the realm of the previously discovered network jets (Kayshap et al., 2018; Tian et al., 2014a). Such explosive events have also been observed as unusual broadening in the Si IV 1402.8 Å line (up to 200 km s^{-1}), and lead to the formation of a flowing cool loop system (Huang et al., 2015; Rao et al., 2019; Srivastava et al., 2020). Observational clues that emerged over the past few years show that the upper chromospheric/TR EEs are ubiquitous in quiet Sun, coronal holes, and in the vicinity of active regions, generating plasma flows (Chen et al., 2019; Huang et al., 2014, 2015; Srivastava et al., 2020). The EEs driven localized plasma flows in the upper chromosphere/TR can transport mass and momentum to the overlying atmosphere, and contribute to the nascent solar wind (Rao et al., 2019). In particular, we focus our attention to cool loop systems for our studies in this thesis and the associated plasma flows.

1.5.2 Active region plasma dynamics underneath solar corona

The bulk mass motions in the loop systems, as captured in the form of Doppler-shift observations, are generally attributed to two kinds of motion, i.e, siphon flows occur due to the pressure difference between the footpoints, and loop filling or draining due to transient heating and subsequent cooling, respectively (Reale, 2014). Also, the persistent redshifts

have been observed in the transition region (TR) in the active regions which are difficult to interpret. The redshifts between 5 and 15 km s^{-1} have been measured accurately from SoHO/SUMER data in solar active regions with little spatial and temporal correlation (Warren et al., 2012). The blueshifts in the transition region (TR) are also studied but not necessarily associated with the coronal loops (Dere et al., 1986). These outflows were found to be related to the EUV explosive events (EEs). However, Teriaca et al. (2003) have thus reported that these EUV explosive events showing blueshifts have chromospheric origin. The transition of redshift to blueshift was also found out in the active region moss, but the transition from red to blue appears to occur at a higher temperature in the moss (1 MK versus 0.5 MK in the quiet Sun) (Dadashi et al., 2012; Tripathi et al., 2012). Coronal plasma motions near footpoints of active region loops showed a strong correlation between Doppler velocity and non-thermal velocity (Tripathi et al., 2012). All these studies have lead to explore their chromospheric counterparts channeling the plasma motions to the corona in confined loop systems. The chromospheric counterparts of these flows have been studied by De Pontieu et al. (2007a) having association to type II spicules which has been explored. But, Madjarska et al. (2011) could not find coronal counterparts to high speed spicules and to be a separate population from lower speed spicules (Zhang et al., 2012). Moreover, IRIS is able to provide more insight into this debatable situation. So, we have explored this gap using different spectral lines from IRIS for our works in the next few chapters. The outline of which is described briefly in the next section.

1.6 Outline of the Thesis

Chapter 2 discusses the basic components of space-based instruments from which the data has been used for our studies. Also, various techniques used to analyze the imaging, magnetic, and spectroscopic data are described.

Chapter 3 depicts dynamics of low-lying cool loop systems using three datasets as observed by the IRIS. We investigate radiances, Doppler shifts and line widths in and around observed cool loop systems using various spectral lines formed between the photosphere and transition region (TR). The inversion of redshift (downflows) to the blueshift (outflows) is firstly observed at C II formation temperature above the footpoint of the cool loop system. This invokes that the impulsive energy release due to small-scale reconnection above loop footpoint seems to be the most likely cause for sudden initiation of the plasma flows evident at TR temperatures. The content of this chapter is partially published in The Astrophysical Journal in 2019.

Chapter 4 describes the modelling of the cool loop systems where the plasma flows are initiated by explosive-events (EEs) at one of its footpoints. The EE causes an unusual broadening of the Si IV 1403 Å line at one of the loop's footpoint. This infers the signature of transient energy release and corresponding velocity enhancement due to EEs that drive further the cool plasma and form the loop system. The data-driven 2D numerical simulation shows that the plasma motions evolve in a similar manner as observed by IRIS in the form of flowing plasma filling a cool-loop system. The main result of this chapter is partially published in The Astrophysical Journal in 2020.

Chapter 5 outlines the observed quiescent coronal loops using multi-wavelength observations from the SDO/AIA on 2016, April 13. The flows at the footpoints of such loop systems are studied using spectral data from IRIS. The Doppler velocity distributions at the footpoints lying in the moss region show the negligible or small flows at Ni I, Mg II k3 and C II line corresponding to upper photospheric and chromospheric emissions. The redshifts (downflows) ranging from 1 to 7 km s^{-1} are observed at Si IV (1393.78 Å ; log(T/K) = 4.8) which is found to be consistent with the existing results regarding dynamical loop systems and moss regions. The results validating the impulsive heating mechanism leading

to plasma flows in quiescent coronal loops. The main content of this chapter is published in Annales Geophysicae Journal in 2019.

Chapter 6, presents a study of an impulsive plasma outflow in the quiet Sun above a plage region using multiwavelength observations from the SDO/AIA having high terminal speed of 1250 km s^{-1}. This plasma ejecta may be caused by the encounter of magnetoacoustic waves with the discontinuity at the X-point that may further develop into the fast magnetic shocks leading to the formation of the observed shock cusp and triggering of the impulsive plasma outflows. The new result of this chapter has been published in the Monthly Notices of the Royal Astronomical Society in 2017.

Chapter 7 discusses the summary and scientific conclusions derived from the various works conducted during the PhD program. The future prospects of these works are also mentioned briefly.